



# Comparison of dedicated breast positron emission tomography and whole-body positron emission tomography/computed tomography images: a common phantom study

Yoko Satoh<sup>1,2</sup> · Utaroh Motosugi<sup>2</sup> · Masamichi Imai<sup>1</sup> · Hiroshi Onishi<sup>2</sup>

Received: 24 September 2019 / Accepted: 14 November 2019 / Published online: 25 November 2019  
© The Japanese Society of Nuclear Medicine 2019

## Abstract

**Objective** High-resolution dedicated breast positron emission tomography (dbPET) can visualize breast cancer more clearly than whole-body PET/computed tomography (CT). In Japan, the combined use of dbPET and whole-body PET/CT is necessary in indications for health insurance. Although several clinical studies have compared both devices, a physical evaluation by the phantom test has not been reported. The aim of this study was to compare the ability of ring-shaped dbPET and whole-body PET/CT using a common phantom with reference to the Japanese guideline for the oncology <sup>18</sup>F-fluorodeoxyglucose (FDG)-PET/CT data acquisition protocol.

**Methods** A cylindrical breast phantom with four spheres of different diameters (16, 10, 7.5, and 5 mm) filled an FDG solution at sphere-to-background radioactivity ratios (SBRs) of 2:1, 4:1, and 8:1 was prepared. Images were then acquired by whole-body PET/CT and subsequently by dbPET. The reconstructed images were visually evaluated and the coefficient of variation and uniformity of the background ( $CV_{\text{background}}$  and  $SD_{\Delta\text{SUV}_{\text{mean}}}$ ), percentages of contrast and background variability ( $\%Q_{\text{H},5\text{mm}}$  and  $\%N_{5\text{mm}}$ ), and their ratio ( $\%Q_{\text{H},5\text{mm}}/N_{5\text{mm}}$ ), and relative recovery coefficient were compared with the standards defined in the protocol for whole-body PET/CT.

**Results** The parameters were calculated at an SBR of 8:1, which was the only SBR in which a 5-mm sphere was visible on both devices. The standards were defined as  $< 10\%$  for  $CV_{\text{background}}$ ,  $\leq 0.025$  for  $SD_{\Delta\text{SUV}_{\text{mean}}}$ ,  $< 5.6\%$  for  $\%N_{5\text{mm}}$ ,  $> 2.8$  for  $\%Q_{\text{H},5\text{mm}}/N_{5\text{mm}}$ , and  $> 0.38$  for the relative recovery coefficient of the smallest sphere (10 mm in diameter) in the protocol for whole-body PET/CT (the  $\%Q_{\text{H},5\text{mm}}$  was not determined for that protocol); the respective values were 6.14%, 0.024, 4.55%, 3.66, and 0.33 for dbPET and 2.21%, 0.021, 3.11%, 1.72, and 0.18 for PET/CT. The  $Q_{\text{H},5\text{mm}}$  was 16.67% for dbPET and 5.34% for PET/CT. The human images also showed higher lesion-to-background contrast on dbPET than on PET/CT despite the noisier background observed with dbPET.

**Conclusion** The common phantom study showed that the background was noisier and that the contrast was much higher in the dbPET image than in the PET/CT image. The acquisition protocol and standards for dbPET will need to be different from those used for whole-body PET/CT.

**Keywords** Dedicated breast positron emission tomography (dbPET) · Whole-body PET/CT · Breast phantom · Image standardization

## Introduction

<sup>18</sup>F-fluorodeoxyglucose (FDG) positron emission tomography/computed tomography (PET/CT) has become one of the most useful tools in diagnostic imaging for cancer. Many studies have demonstrated the efficacy of whole-body FDG-PET/CT in staging or re-staging, in monitoring the response to therapy, and for prediction of the prognosis in patients with breast cancer [1–3]. It is important to detect breast cancer at an early stage when it is small, given that mortality increases

✉ Yoko Satoh  
ysatoh@ypic.jp

<sup>1</sup> Yamanashi PET Imaging Clinic, Shimokato 3046-2, Chuo, Yamanashi 409-3821, Japan

<sup>2</sup> Department of Radiology, University of Yamanashi, Chuo, Yamanashi, Japan

with tumors exceeding 1 cm in size [4, 5]. However, detection of small breast cancers by whole-body PET/CT is challenging, because of its limited spatial resolution [6].

High-resolution dedicated breast PET (dbPET) scanners have been developed to detect small breast lesions. There are two types of high-resolution dbPET, i.e., positron emission mammography (PEM) and a tomographic technique using a ring-shaped scanner (ring-shaped dbPET) [7]. PEM systems depict breast tissue via soft compression of the breast with two opposing plate-like detectors and have higher sensitivity than whole-body PET/CT [8–10], while ring-shaped dbPET scanners can visualize breast cancer more clearly than whole-body PET/CT [11, 12]. These high-resolution breast PET systems have greater photon sensitivity and can improve spatial resolution by setting the detector close to the breast, reducing respiratory movement, and using smaller detection units with reconstruction methods that are different to those used for whole-body PET/CT. In Japan, combined use of dbPET and whole-body PET/CT is necessary in some indications for health insurance and the Japanese Society of Nuclear Medicine also recommends their combined use [13]. dbPET can evaluate local lesions of breast cancer, which is difficult to do by whole-body PET due to its spatial resolution limitations. Conversely, whole-body PET can scan for metastasis, including the lymph nodes, which cannot be evaluated by dbPET. Therefore, a more accurate diagnosis can be achieved using both modalities, rather than one examination, which would lead to the selection of an appropriate treatment method and improvement of the prognosis of the breast cancer patient.

The standard performance of dbPET has been evaluated previously using a rat-sized phantom [NU4-2008, National Electrical Manufacturers Association (NEMA), Rosslyn, VA, USA] [14, 15]. Furthermore, a phantom experiment procedure manual for the NEMA NU-2 2007, a body phantom, has been created for standardization of whole-body PET images in Japan [16]. The spatial resolution of most whole-body PET scanners is approximately 5 mm [17, 18], whereas that of a dbPET system is approximately 2 mm [14]. Although combined use of dbPET and whole-body PET/CT is recommended; the performance of these devices when using a common phantom has not been reported. Therefore, the purpose of this phantom study based on the Japanese FDG-PET/CT data acquisition protocol was to demonstrate and compare the performance of high-resolution dedicated breast positron emission tomography (dbPET) with whole-body PET/CT.

## Materials and methods

### Ring-shaped dbPET scanner

The ring-shaped dbPET scanner (Elmammo, Shimadzu Corp., Kyoto, Japan) consists of 36 detector modules

arranged in three contiguous rings, has a diameter of 195 mm and an axial length of 156.5 mm, and has depth-of-interaction measurement capability [19]. The transaxial effective field-of-view (FOV) is  $185 \times 156.5 \text{ mm}^2$ . Each detector block consists of a four-layered  $32 \times 32$  array of lutetium oxyorthosilicate crystals coupled to a 64-channel positron-sensitive photomultiplier tube via a light guide. Attenuation correction was calculated using a uniform attenuation map with object boundaries obtained from emission data [20] and scatter corrections were applied for all images. Scatter correction was performed using the convolution-subtraction method [21] with kernels obtained by background tail fitting. Performance metrics included 1.5-mm FWHM resolution in standard mode in the axial, sagittal, and coronal views, detector sensitivity of 0.09–0.13 cps/Bq at the center of the detector, and detector sensitivity of 0.05–0.08 cps/Bq at a quarter depth of the detector. The peak noise equivalent count was 600–800 kcps. The characteristics of this scanner have been reported in detail previously [14]. The standard performances are shown in Table 1.

### Whole-body PET/CT scanner

PET/CT scans were obtained using a Biograph Horizon TrueV FDG-PET/CT system (Siemens Medical Solutions, Knoxville, TN, USA). This system has 52 detector rings consisting of 160 blocks, with each block containing an array of  $13 \times 13$  lutetium oxyorthosilicate crystals ( $4 \text{ mm} \times 4 \text{ mm} \times 20 \text{ mm}$ ) covering an axial FOV of 221 mm and having a transaxial FOV of 690 mm. The coincidence timing window and time-of-flight system timing resolution were 4.1 ns and 540 ps, respectively. A CT scan was performed for attenuation correction (130 kV; 15–70 mA; tube

**Table 1** Standard performances of dbPET and PET/CT

	dbPET <sup>a</sup>	PET/CT <sup>b</sup>
Spatial resolution		
Transverse axial	@5 mm < 1.5 FWHM	@10 mm 4.3 FWHM
Transverse tangential	@5 mm < 1.5 FWHM	@10 mm 4.7 FWHM
Sensitivity		
cps/kBq	90–130	11.7
Peak NECR		
kcps	350–550	155
kBq/ml	80–150	26

FWHM full width at half maximum, dbPET dedicated breast positron emission tomography, NECR peak noise equivalent count, PET/CT positron emission tomography

<sup>a</sup>Provided by Shimadzu Corp

<sup>b</sup>Provided by Siemens Medical Solutions. These values are based on the results of analyses using a <sup>22</sup>Na point source and a NU4-2008 phantom (National Electrical Manufacturers Association) (a), and a <sup>68</sup>Ge point source and NU2-2012 (b)

rotation time, 0.6 s per rotation; pitch, 1; a transaxial FOV, 700 mm; and section thickness, 5 mm). The standard performances are shown in Table 1.

## Development and preparation of the breast phantom

A cylindrical breast phantom made of acrylic resin was used to compare the detectability of lesions on dbPET with that on PET/CT (Fig. 1). The phantom was constructed to contain four plastic spheres of different diameters. The inner and outer diameters of the cylinder were 100 mm and 140 mm, respectively, and the height was 170 mm. The diameters of the spheres arranged inside were 5, 7.5, 10, and 16 mm. The cylinder and four spheres were filled with  $^{18}\text{F}$ -FDG solution at sphere-to-background radioactivity ratios (SBRs) of 8:1, 4:1, and 2:1 to account for the fact that FDG uptake in the mammary gland is physiologically variable according to age, the amount of fibroglandular tissue, and the menstrual cycle, ranging from  $\text{SUV}_{\text{max}}$  0.65 to 2.05 [22, 23]. The background radioactivity at the start of data acquisition by PET/CT and dbPET was set to 3.01 and 2.46 kBq/mL, respectively. The phantom was prepared in these three conditions separately. One scan was performed under each condition. The phantom was placed in the detector, so that the spheres were located at the center plane of the detector. Sphere placement at the center of the detector was confirmed visually on the image.

## Data acquisition and image reconstruction

The phantom was placed at the center of the column in the dbPET or PET/CT detector, so that the four spheres were aligned horizontally and then scanned by both devices for 20 min in list mode. The dbPET images were reconstructed using a three-dimensional list mode dynamic row-action

maximum-likelihood algorithm with one iteration and 128 subsets, a relaxation control parameter of  $\beta=20$ , a matrix size in the axial view of  $236 \times 200 \times 236$  with a post-reconstruction smoothing Gaussian filter (1.17 mm FWHM), and scatter correction. The PET/CT images were reconstructed using the ordered subset expectation maximization method and the time-of-flight algorithm with four iterations and ten subsets. The CT data were resized from a  $512 \times 512$  matrix to a  $180 \times 180$  matrix to match the PET data and construct CT-based transmission maps for attenuation correction of the PET data with a post-reconstruction smoothing Gaussian filter (5 mm FWHM). These conditions were determined based on those used in a previous study using dbPET [24].

## Analyses of phantom image quality

Visual analyses of the phantom images were performed using syngo. via VB10 (Siemens Healthcare GmbH, Erlangen, Germany). An experienced nuclear medicine physician and two experienced PET technologists evaluated the hot spheres. Evaluations were performed using the slices displayed in the transverse image slice containing the centers of the spheres. The images were displayed in an inverse gray scale with a standardized uptake range of 0–6. The hot sphere of 5 mm in diameter was visually graded as follows: 2, identifiable; 1, visualized, but similar hot spots observed elsewhere; and 0, not visualized. Spheres with visual scores  $\geq 1.5$  were deemed to be detectable. The final score was the mean of the scores from three readers. The visual assessment was performed based on the Japanese guideline [13]. It was decided by consensus that the SBR was suitable for physical analysis.

The physical analysis was also performed using syngo. via VB10. According to the Japanese guideline for the FDG-PET/CT oncology data acquisition protocol, dbPET image quality was also analyzed using the parameters described below. The three formulas were modified from those described in the standard PET imaging protocols and phantom test procedures and criteria [25].

The coefficient of variation and uniformity of the background ( $\text{CV}_{\text{background}}$  and  $\text{SD}_{\Delta\text{SUV}_{\text{mean}}}$ , respectively) were calculated by evaluation of various regions of interest (ROIs) in the transverse image slice that contained the centers of the spheres. Ten ROIs with a diameter of 16 mm were placed in the background region in that slice and adjacent  $\pm 5$  mm and 10 mm slices (50 ROIs in total), as illustrated in Fig. 2a.

$\text{CV}_{\text{background}}$  and  $\text{SD}_{\Delta\text{SUV}_{\text{mean}}}$  were calculated using the following:

$$\text{CV}_{\text{background}} = \text{mean of} \left[ \frac{\text{SD}_{16\text{mm}}}{C_{\text{B},16\text{mm}}} \times 100 \right] (\%)$$

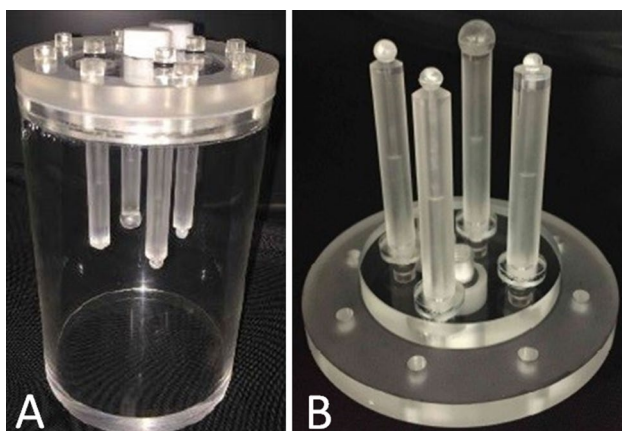


**Fig. 1** Cylindrical breast phantom. A cylindrical breast phantom consisting of an outer cylinder (a) and four spheres of different diameter (5, 7.5, 10, and 16 mm) (b)

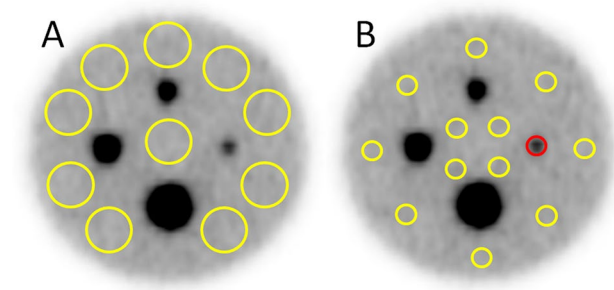


**Fig. 2** Positioning of the regions of interest for the analyses of image quality. Regions of interest measuring 16 mm diameter were placed over the phantom background (yellow) of the reconstructed PET images at a sphere-to-background radioactivity ratio of 8:1 and were used for analysis of  $CV_{\text{background}}$  and  $SD_{\Delta\text{SUV}_{\text{mean}}}$  (a). Regions of interest measuring 5 mm diameter were placed over the smallest active sphere (red) and the phantom background (yellow) of the reconstructed PET images at a sphere-to-background radioactivity ratio of 8:1 and were used for analysis of  $\%Q_{\text{H},5\text{mm}}$  and  $\%N_{5\text{mm}}$  (b). PET positron emission tomography

$$SD_{\Delta\text{SUV}_{\text{mean}}} = \sqrt{\frac{1}{n} \sum_{i=1}^n (\Delta\text{SUV}_{\text{mean},i})^2}$$

$SD_{16\text{mm}}$  is the standard deviation of the background ROI values that was 16 mm in diameter,  $C_{\text{B},16\text{mm}}$  is the average of the background ROI values that was 16 mm in diameter,  $\Delta\text{SUV}_{\text{mean},i}$  is the relative error of each background ROI value that was 16 mm in diameter.  $n$  is 50 which is the sum of 10 ROIs set for each slice.

The percentages of contrast and background variability ( $\%Q_{\text{H},5\text{mm}}$  and  $\%N_{5\text{mm}}$ ) and their ratio ( $\%Q_{\text{H},5\text{mm}}/N_{5\text{mm}}$ ) were also calculated by evaluation of various ROIs. The 12 ROIs that were 5 mm in diameter were placed on the background region in that slice and adjacent  $\pm 5$  mm and 10 mm slices (60 ROIs in total) as illustrated in Fig. 2b.  $\%Q_{\text{H},5\text{mm}}$  and  $\%N_{5\text{mm}}$  were used as a measure for the image contrast and noise for sphere and their ideal values were 100 and 0%, respectively.

$\%Q_{\text{H},5\text{mm}}$  was calculated using the following:

$$\%Q_{\text{H},5\text{mm}} = \frac{C_{\text{H},5\text{mm}}/C_{\text{B},5\text{mm}} - 1}{a_{\text{H}}/a_{\text{B}} - 1} \times 100(\%)$$

$C_{\text{H},5\text{mm}}$  is the average pixel value in the ROI for the 5-mm sphere,  $C_{\text{B},5\text{mm}}$  is the average pixel value in the background regions of all ROIs,  $a_{\text{H}}$  is the measured activity concentration in the hot spheres,  $a_{\text{B}}$  is the measured activity concentration in the background.

In addition,  $\%N_{5\text{mm}}$  was calculated using the following:

$$\%N_{5\text{mm}} = \frac{SD_{5\text{mm}}}{C_{\text{B},5\text{mm}}} \times 100(\%)$$

$$SD_{5\text{mm}} = \sqrt{\frac{\sum_{k=1}^{60} (C_{\text{B},5\text{mm},k} - C_{\text{B},5\text{mm}})^2}{(60 - 1)}}$$

$SD_{5\text{mm}}$  is the standard deviation of the background ROI values for a 5-mm-diameter sphere,  $C_{\text{B},5\text{mm}}$  is the average pixel value in the background regions of all ROIs, The ratio of  $\%Q_{\text{H},5\text{mm}}$  and  $\%N_{5\text{mm}}$  (QNR) was also calculated:

$$\text{QNR} = \%Q_{\text{H},5\text{mm}}/\%N_{5\text{mm}}$$

The recovery coefficient (RC) was defined as the ratio of the measured sphere activity to the true sphere activity. The  $\text{SUV}_{\text{max}}$  of the four hot spheres was determined from a circular ROI placed on the center slice of the images of each sphere. The diameter of each ROI was equal to that of each sphere (5, 7.5, 10, and 16 mm).

The relative RC was calculated using the following:

$$\text{RC}_j = C_j/C_{16\text{mm}}$$

$C_j$  is the  $\text{SUV}_{\text{max}}$  of each ROI in each sphere,  $C_{16\text{mm}}$  is the  $\text{SUV}_{\text{max}}$  of the ROI with a 16-mm diameter for a sphere with a 16-mm diameter.

## Human imaging

Patients fasted at least 6 h prior to administration of  $^{18}\text{F}$ -FDG (3 MBq/kg) and were scanned by whole-body PET/CT for 90 s per bed and dbPET for 7 min per breast. Scans were performed at 60-min and 90-min post injection, both in the prone position.

The PET/CT and dbPET images were reconstructed using the same conditions as for the phantom images. The  $\text{SUV}_{\text{max}}$  of the abnormal FDG uptake and  $\text{SUV}_{\text{mean}}$  of the normal background were measured. To measure the  $\text{SUV}_{\text{mean}}$  of the background, a VOI with a diameter of approximately 2–2.5 cm was placed on the contralateral normal mammary gland, avoiding structures such as the nipple and the chest wall. The size of the VOI on the background varied slightly depending on the volume of the mammary gland in each patient. Where patients had previously undergone unilateral mastectomy, a VOI was placed on the ipsilateral mammary gland as far as possible from the abnormal uptake. Two representative cases were shown in this study.

This component of the study was approved by our institutional review board and written informed consent was obtained from the study participants.



## Results

The visual scores on the dbPET and PET/CT images were, respectively, 0 and 0 for an SBR of 2:1, 1 and 0 for an SBR of 4:1, and 2 and 0.7 for an SBR of 8:1 (Table 2). Representative phantom images acquired by the two scanners for various SBRs and their three-dimensional pixel maps at an SBR of 8:1 are shown in Fig. 3.

The  $CV_{\text{background}}$ ,  $SD_{\Delta\text{SUVmean}}$ , and  $\%N_{5\text{mm}}$  values on the images scanned by dbPET and PET/CT were 6.14 and 2.21, 0.024 and 0.021, and 4.55 and 3.11, respectively. The  $CV_{\text{background}}$  and  $\%N_{5\text{mm}}$  values on dbPET were higher than those on PET/CT; in contrast, the  $\%Q_{\text{H},5\text{mm}}$  values were 16.67 and 5.34, respectively, and the  $\%Q_{\text{H},5\text{mm}}/\%N_{5\text{mm}}$  values were 3.66 and 1.72 (Table 2). The RCs for the 5-mm sphere on dbPET and PET/CT were 0.33 and 0.18, respectively (Fig. 4).

Figure 5 shows representative clinical images acquired by dbPET and PET/CT in the prone position. The focal FDG uptakes were visualized on both dbPET and PET/CT images. However, they had clearer and more obvious on dbPET, despite the degree of background FDG uptake by the mammary gland.

## Discussion

In this study, we investigated the difference in quality of a common breast phantom and clinical images between dbPET and whole-body PET/CT to define the parameters needed to standardize dbPET images according to the Japanese protocol for whole-body PET/CT.

In the phantom study, although there was no significant difference in uniformity ( $SD_{\Delta\text{SUVmean}}$ ) between dbPET and whole-body PET/CT, the  $CV_{\text{background}}$  and  $\%N_{5\text{mm}}$

values were higher on dbPET than on whole-body PET/CT (Table 2), indicating that the background on dbPET was noisier than that on whole-body PET, as shown in the phantom images (Fig. 3) and clinical images (Fig. 5). Despite the noisier background, the  $\%Q_{\text{H},5\text{mm}}$  and  $\%Q_{\text{H},5\text{mm}}/\%N_{5\text{mm}}$  values on dbPET were much higher than those on whole-body PET/CT (Table 2). This finding means that the lesion-to-background contrast of dbPET was better than that of whole-body PET/CT, which is consistent with previous reports [10, 26]. Furthermore, the RCs for the smaller spheres were higher on dbPET than on PET/CT, indicating that the partial volume effect of dbPET was less than that of PET/CT. These results demonstrate that dbPET delineates lesions about 5 mm in size more clearly than whole-body PET/CT.

In this study, we referenced the whole-body FDG-PET/CT data acquisition protocol for oncology that is designed to standardize PET/CT images in Japan. However, there is no dbPET imaging protocol at present. The protocol for PET/CT recommends the use of the NEMA NU-2 2007, a widely used body phantom, with an SBR of 4:1 for acquisition. The NU-2 2007 contains six spheres with diameters of 32, 28, 22, 17, 13, and 10 mm. There were some differences in the phantom used in the whole-body PET/CT protocol and that used in our study in terms of the size of the sphere, a suitable SBR, and acquisition time. Moreover, given that the acquisition time that is considered clinically acceptable differs between dbPET and whole-body PET/CT, a different PET/CT protocol for the phantom test will be needed for standardization of the dbPET images.

In the PET/CT protocol devised for oncology, the standard values recommended for the physical indicators are as follows:  $SD_{\Delta\text{SUVmean}} < 10\%$ ;  $SD_{\Delta\text{SUVmean}} < 0.025$ ;  $\%N_{10\text{mm}} < 5.6\%$ ;  $\text{QNR} > 2.8$ ; and  $\text{RC}_{10\text{mm}} > 0.38$ . It is noteworthy that a standard value for  $\%Q_{\text{H}}$  is not defined in the guideline for whole-body PET/CT. It is important for detection of a lesion by whole-body PET/CT that  $\%N$

**Table 2** Results of the phantom image quality analyses

Visual assessment	dbPET			PET/CT		
	2:1	4:1	8:1	2:1	4:1	8:1
SBR	2:1	4:1	8:1	2:1	4:1	8:1
Score (average)	0	1	2	0	0	0.7
$CV_{\text{background}}^a$	6.14			2.21		
$SD_{\Delta\text{SUVmean}}^a$	0.024			0.021		
$\%N_{5\text{mm}}^a$	4.55			3.11		
$\%Q_{\text{H},5\text{mm}}^a$	16.67			5.34		
$\%Q_{\text{H},5\text{mm}}/\%N_{5\text{mm}}^a$	3.66			1.72		

All parameters<sup>a</sup> were calculated at an SBR of 8:1

dbPET dedicated breast positron emission tomography, PET/CT positron emission tomography, SBR sphere-to-background ratio,  $CV_{\text{background}}$  the coefficient of variation of the background,  $SD_{\Delta\text{SUVmean}}$  the uniformity of the background,  $\%N_{5\text{mm}}$  the percentage of the background variability,  $\%Q_{\text{H},5\text{mm}}$  the percentage of the contrast

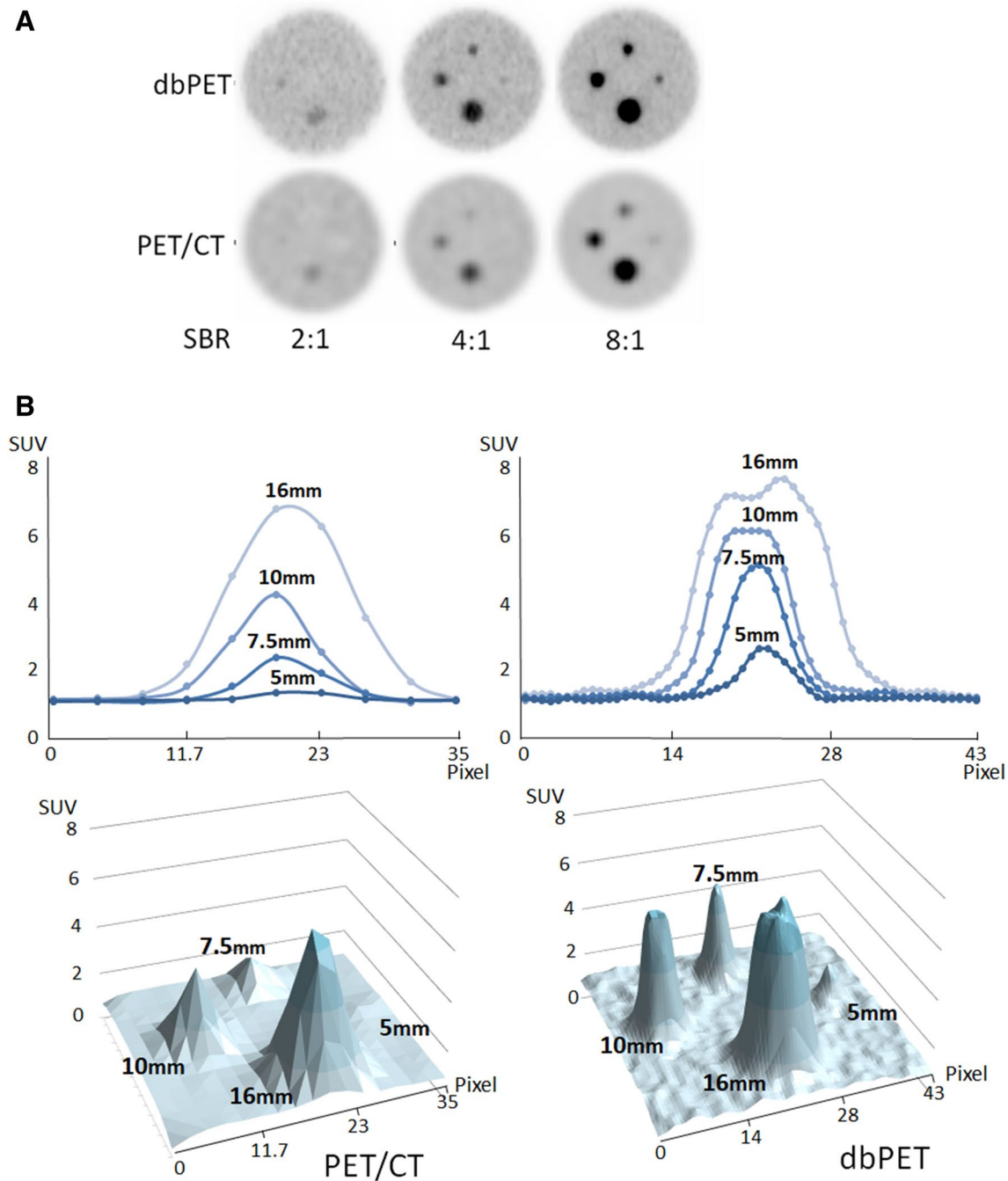


**Fig. 3** Images of the breast phantom scanned by dbPET and PET/CT. The background on dbPET was noisier than that on PET/CT. However, the hot spots were more clearly visualized. The smallest spheres were visible, so the physical assessment was made with an SBR of 8:1 (a). Two- and three-dimensional pixel maps for four spheres (5, 7.5, 10, and 16 mm in diameters) of the breast phantom images

scanned at a SBR of 8:1 also showed that the background on dbPET is rougher, but the hotspots are more sharply delineated on dbPET than on PET/CT (b). *dbPET* dedicated breast positron emission tomography, *PET/CT* positron emission tomography, *SBR* sphere-to-background ratio

is sufficiently small [13]. In contrast, despite the  $%N$  for dbPET being higher than that for PET/CT, the  $%Q_H$  was much higher for dbPET, resulting in a higher QNR and a high-contrast image. It seems that a high  $%Q_H$  is more important for detection of lesions in dbPET images. Given

these results, standard index values that are different from those for PET/CT will be needed for dbPET.

We evaluated both dbPET and whole-body PET/CT using a common breast phantom. Currently, not only ring-shaped dbPET, but also different types of PEM devices

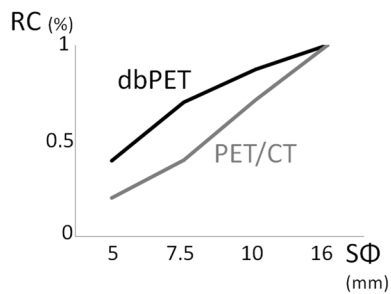


**Fig. 4** Recovery coefficients for four spheres on dbPET and PET/CT. Recovery coefficients measured for different sphere sizes. Images with 20 min of acquisition were used. *dbPET* dedicated breast positron emission tomography, *PET/CT* positron emission tomography, *RC* recovery coefficient, *SUV* standardized uptake value

are commercially available and used. However, there is no acquisition protocol for a test using a common phantom. In the case of PET/CT, although the specifications of the detector and the image reconstruction method are different, the

shape of the detectors and the images obtained are almost the same for each device. Therefore, standardization of the imaging methods for whole-body PET/CT can be performed by a test using the same phantom with physical and visual assessments. However, there are two types of high-resolution breast PET, i.e., dbPET, which has a ring-shaped detector, and PEM, which has two plate-like detectors with markedly different shapes, so it is difficult to standardize images obtained from these devices by a test using the same phantom. A previous study evaluated dbPET (MAMMI breast PET, Oncovision, Valencia, Spain) and whole-body PET/CT using a specially made phantom containing gelatin and hydrogel [27] that would be difficult to use repeatedly in a multicenter setting. A common phantom with the durability and reproducibility like the NEMA body phantom would be preferable. Furthermore, standardization of quantitiveness is also a problem, because the quantification method varies depending on the device.

The harmonization of quantitative PET parameters is necessary to use them for diagnostic, prognostic, or therapeutic

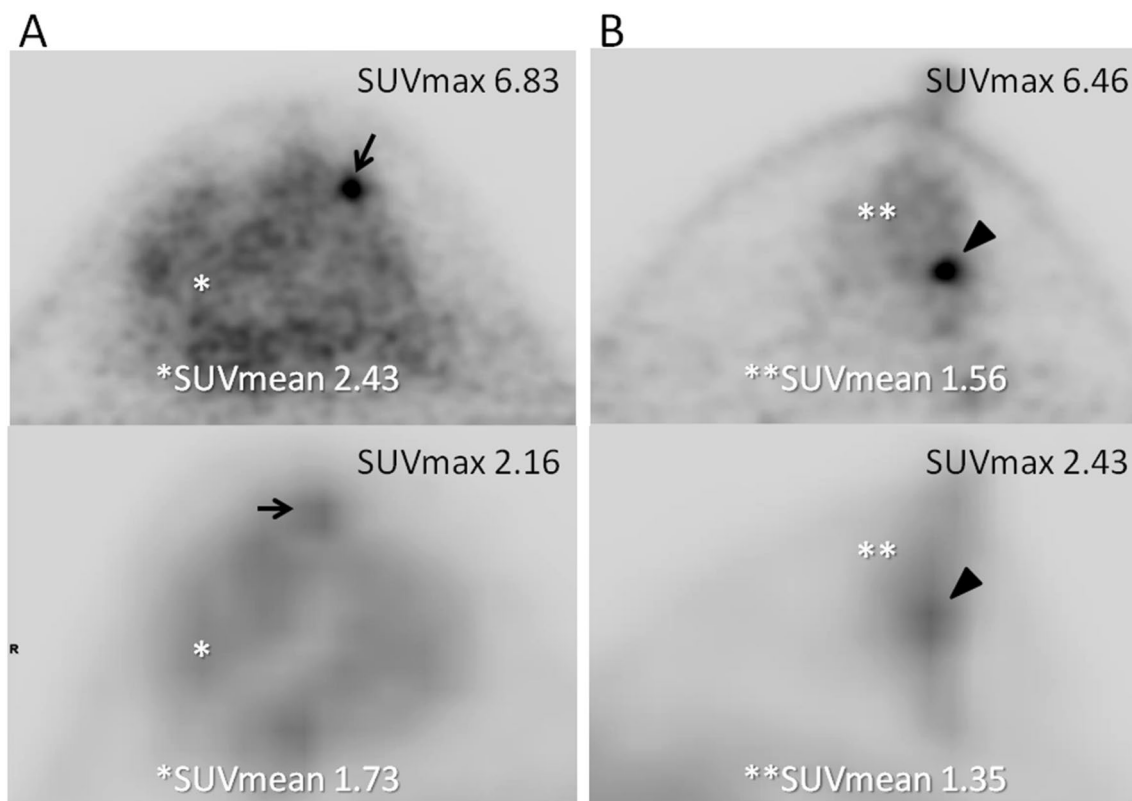


**Fig. 5** Clinical images of dbPET and PET/CT. Representative clinical images of dbPET (upper) and PET/CT (lower) with higher (case A) and lower (case B) focal FDG uptake in the background mammary gland tissue. The focal uptakes were visualized on both the dbPET and PET/CT images. However, they were clearer and more obvious on dbPET and showed more contrast despite the degree of FDG uptake in the background mammary gland tissue (asterisk in **a**,

double asterisk in **b**). **a** Image from a 52-year-old woman. The focal FDG uptake corresponded to a 4-mm mass (BI-RADS category 3) on ultrasonography. **b** Image from a 41-year-old woman. The focal FDG uptake corresponded to a 4-mm enhanced mass (BI-RADS category 3) on magnetic resonance imaging. *BI-RADS* Breast Imaging Reporting and Data System, *FDG*  $^{18}\text{F}$ -fluorodeoxyglucose

monitoring, regardless of the scanners [28]. In Japan, some standard physical indicators of whole-body PET/CT images have been defined and phantom test procedures also have been established [16, 25]. Currently, there are two types of commercially available high-resolution breast PET: dbPET and PEM, which have detectors with significantly different shapes. The next challenge is how to harmonize these scanners; however, harmonization will be very difficult to achieve for breast PET due to the large number of differences in the quantification methods of these two types of breast PET scanners. It would be appropriate to define some standards such as a recovery coefficient, to provide relative values, and to standardize the image using a common phantom, which can be scanned with both scanners. As with whole-body PET/CT, the breast PET imaging guidelines and the phantom test procedure should also be published.

This study has some limitations. First, to evaluate the standard performance of dbPET and to compare it with PET/CT, the phantoms were scanned at the center of the ring-shaped detector, as in a previous report [14]. However, many Japanese women have small breasts and their mammary glands are often located near the chest wall above the center of the detector even if they are in the prone position. This tendency is particularly common in young women, who are less likely to have breast ptosis than older women. Therefore, the position of the phantom in the detector needs to be changed more often. Second, we did not consider the optimal reconstruction conditions for dbPET; unlike with phantom images, it may be necessary to consider other factors when examining clinical images such as physical uptake in the mammary gland, heart, and pectoral muscles. Third, the phantom was scanned only once for each condition. It would have been better in terms of reproducibility to calculate the average results of several scans under each condition.

## Conclusion

This phantom study showed that the background was noisier and that the contrast was much higher in dbPET images than in PET/CT images. The acquisition protocol and standards for dbPET will need to be different from those used for whole-body PET/CT. Standardization of the quantitative evaluation of dbPET will enable more accurate assessment of treatment effects and prognosis prediction.

## References

- Groheux D, Espie M, Giacchetti S, Hindie E. Performance of FDG PET/CT in the clinical management of breast cancer. *Radiology*. 2013;266:388–405.
- Lee SM, Bae SK, Kim TH, Yoon HK, Jung SJ, Park JS, et al. Value of 18F-FDG PET/CT for early prediction of pathologic response (by residual cancer burden criteria) of locally advanced breast cancer to neoadjuvant chemotherapy. *Clin Nucl Med*. 2014;39:882–6.
- Satoh Y, Nambu A, Ichikawa T, Onishi H. Whole-body total lesion glycolysis measured on fluorodeoxyglucose positron emission tomography/computed tomography as a prognostic variable in metastatic breast cancer. *BMC Cancer*. 2014;14:525.
- Saadatmand S, Bretveld R, Siesling S, Tilanus-Linthorst MM. Influence of tumor stage at breast cancer detection on survival in modern times: population based study in 173,797 patients. *BMJ*. 2015;351:h4901.
- Ichizawa N, Fukutomi T, Iwamoto E, Akashi-Tanaka S. Long-term results of T1a, T1b and T1c invasive breast carcinomas in Japanese women: validation of the UICC T1 subgroup classification. *Jpn J Clin Oncol*. 2002;32:108–9.
- Kumar R, Chauhan A, Zhuang H, Chandra P, Achnall M, Alvavi A. Clinicopathologic factors associated with false negative FDG-PET in primary breast cancer. *Breast Cancer Res Treat*. 2006;98:267–74.
- Bowen SL, Wu Y, Chaudhari AJ, Fu L, Packard NJ, Burkett GW, et al. Initial characterization of a dedicated breast PET/CT scanner during human imaging. *J Nucl Med*. 2009;50:1401–8.
- Fowler AM. A molecular approach to breast imaging. *J Nucl Med*. 2014;55:177–80.
- Kalinyak JE, Berg WA, Schilling K, Madsen KS, Narayanan D, Tartar M. Breast cancer detection using high-resolution breast PET compared to whole-body PET or PET/CT. *Eur J Nucl Med Mol Imaging*. 2014;41:260–75.
- Yamamoto Y, Ozawa Y, Kubouchi K, Nakamura S, Nakajima Y, Inoue T. Comparative analysis of sensitivity of positron emission mammography and whole-body PET in relation to tumor size. *Clin Nucl Med*. 2015;40:21–5.
- Nishimatsu K, Nakamoto Y, Miyake KK, Ishimori T, Kanao S, Toi M, et al. Higher breast cancer conspicuity on dbPET compared to WB-PET/CT. *Eur J Radiol*. 2017;90:138–45.
- Nakamoto R, Nakamoto Y, Ishimori T, Nishimatsu K, Miyake KK, Kanao S, et al. Diagnostic performance of a novel dedicated breast PET scanner with C-shaped ring detectors. *Nucl Med Commun*. 2017;38:388–95.
- Hosono M, Saga T, Ito K, Kumita S, Sasaki M, Senda M, et al. Clinical practice guideline for dedicated breast PET. *Ann Nucl Med*. 2014;28:597–602.
- Miyake KK, Matsumoto K, Inoue M, Nakamoto Y, Kanao S, Oishi T, et al. Performance evaluation of a new dedicated breast PET scanner using NEMA NU4-2008 standards. *J Nucl Med*. 2014;55:1198–203.
- Mitsumoto T, Uno K, Irie M, Wu J, Sasamori H, Tsuchiya Y, et al. The potential of dedicated breast PET with a ring-type scanner—basic evaluation and clinical experience. *Radioisotopes*. 2018;67:309–19.
- Fukukita H, Suzuki K, Matsumoto K, Terauchi T, Daisaki H, Ikari Y, et al. Japanese guideline for the oncology FDG-PET/CT data acquisition protocol: synopsis of Version 2.0. *Ann Nucl Med*. 2014;28:693–705.
- MacDonald L, Edwards J, Lewellen T, Rogers J, Kinahan P. Clinical imaging characteristics of the positron emission mammography PEM Flex Solo II. *IEEE Nucl Symp Conf Rec*. 2008;11:4494–501.
- Raylman RR, Abraham J, Hazard H, Koren C, Filburn S, Schreiman JS, et al. Initial clinical test of a breast PET scanner. *J Med Imaging Radiat Oncol*. 2011;55:58–64.
- Qi J, Kuo C, Huesman RH, Klein GJ, Moses WW, Reutter BW. Comparison of rectangular and dual-planar positron emission mammography scanners. *IEEE Trans Nucl Sci*. 2002;49:2089–96.
- Yamakawa Y, Kitamura K. Attenuation correction using level set method for application specific PET scanners. In: Nuclear science



- symposium and medical imaging conference (NSS/MIC) IEE. pp 3130–2; 2011.
21. Bailey DL, Meikle SR. A convolution-subtraction scatter correction method for 3D PET. *Phys Med Biol.* 1994;39:411–24.
  22. Park HH, Shin JY, Lee JY, Jin GH, Kim HS, Lyu KY, et al. Discussion on the alteration of 18F-FDG uptake by the breast according to the menstrual cycle in PET imaging. *Conf Proc IEEE Eng Med Biol Soc.* 2013;2013:2469–72.
  23. Leithner D, Baltzer PA, Magometschnigg HF, et al. Quantitative assessment of breast parenchymal uptake on 18F-FDG PET/CT: correlation with age, background parenchymal enhancement, and amount of fibroglandular tissue on MRI. *J Nucl Med.* 2016;57:1518–22.
  24. Satoh Y, Motosugi U, Omiya Y, Onishi H. Unexpected abnormal uptake in the breasts at dedicated breast PET: incidentally detected small cancers or nonmalignant features? *AJR Am J Roentgenol.* 2019;212:443–9.
  25. Phantom test procedure for whole body PET imaging using 18F-FDG, 3rd ed. Japanese Society of Nuclear Medicine, PET Nuclear Medicine Committee; 2017.
  26. Yamamoto Y, Tasaki Y, Kuwada Y, Ozawa Y, Inoue T. A preliminary report of breast cancer screening by positron emission mammography. *Ann Nucl Med.* 2016;30:130–7.
  27. García Hernández T, Vicedo González A, Ferrer Rebolleda J, Sánchez Jurado R, Roselló Ferrando J, Brualla González L, et al. Performance evaluation of a high resolution dedicated breast PET scanner. *Med Phys.* 2016;43:2261–72.
  28. Makris NE, Huisman MC, Kinahan PE, Lammertsma AA, Boellaard R. Evaluation of strategies towards harmonization of FDG PET/CT studies in multicentre trials: comparison of scanner validation phantoms and data analysis procedures. *Eur J Nucl Med Mol Imaging.* 2013;40:1507–15.

**Publisher's Note** Springer Nature remains neutral with regard to jurisdictional claims in published maps and institutional affiliations.